

Supplemental Information

Adsorption variations on Ni (111) surface: electron density diversity from
oxygen-containing functional groups

Changwei Liu^{1#}, Congtao Wen^{4#}, Zekai Zhang², Yuxin Chen¹, Huachao Yang³, Jia-hui Li^{2*},

Cheng Lian^{1,2*}, Honglai Liu^{1,2}

¹State Key Laboratory of Chemical Engineering, Shanghai Engineering Research Center of Hierarchical Nanomaterials, School of Chemical Engineering, East China University of Science and Technology, Shanghai, 200237, China

²School of Chemistry and Molecular Engineering, East China University of Science and Technology, Shanghai, 200237, China

³State Key Laboratory of Clean Energy Utilization, College of Energy Engineering, Zhejiang University, Hangzhou 310027, China

⁴College of Life and Environmental Sciences, Wenzhou University, Wenzhou 325035, China

* Corresponding Author. E-mail address: J-H. Li at jiahuili@ecust.edu.cn and C. Lian at lian Cheng@ecust.edu.cn.

Table of Contents

| | |
|--|-----|
| Table S1. Calculated adsorption energies for oxygen-containing organic monomers on Ni(111) surfaces relative to gas-phase compounds in this work and previous studies. | S13 |
| Figure S1. Possible adsorption sites of Guaiacol compound at the Ni (111) surface. | S3 |
| Figure S2. The radial distribution function of the optimal adsorption configuration of aromatic hydrocarbon benzene ring carbon atoms on the surface, guaiacol, toluene, and catachol. | S4 |
| Figure S3. Possible adsorption sites of toluene compound and corresponding adsorption energies at the Ni (111) surface. | S5 |
| Figure S4. Possible adsorption sites of catechol compound and corresponding adsorption energies at the Ni (111) surface. | S6 |
| Figure S5. Possible adsorption sites of acetic acid compound and corresponding adsorption energies at the Ni (111) surface. | S7 |
| Figure S6. Possible adsorption sites of methyl acetate compound and corresponding adsorption energies at the Ni (111) surface. | S8 |
| Figure S7. Possible adsorption sites of N-butanol compound and corresponding adsorption energies at the Ni (111) surface. | S9 |
| Figure S8. Possible adsorption sites of N-hexanal compound and corresponding adsorption energies at the Ni (111) surface. | S10 |
| Figure S9. Possible adsorption sites of cyclopentanedione compound and corresponding adsorption energies at the Ni (111) surface. | S11 |
| Figure S10. Calculated electron localization function (ELF) of polarized Ni atoms for different adsorption systems. | S12 |
| Figure S11. Calculated Electron density difference (EDD) (left maps), total density of states (TDOS) of the pure-substrates and adsorbates, and partial density of states (PDOS) of the Ni atoms that lose the most electrons (right curves). | S14 |

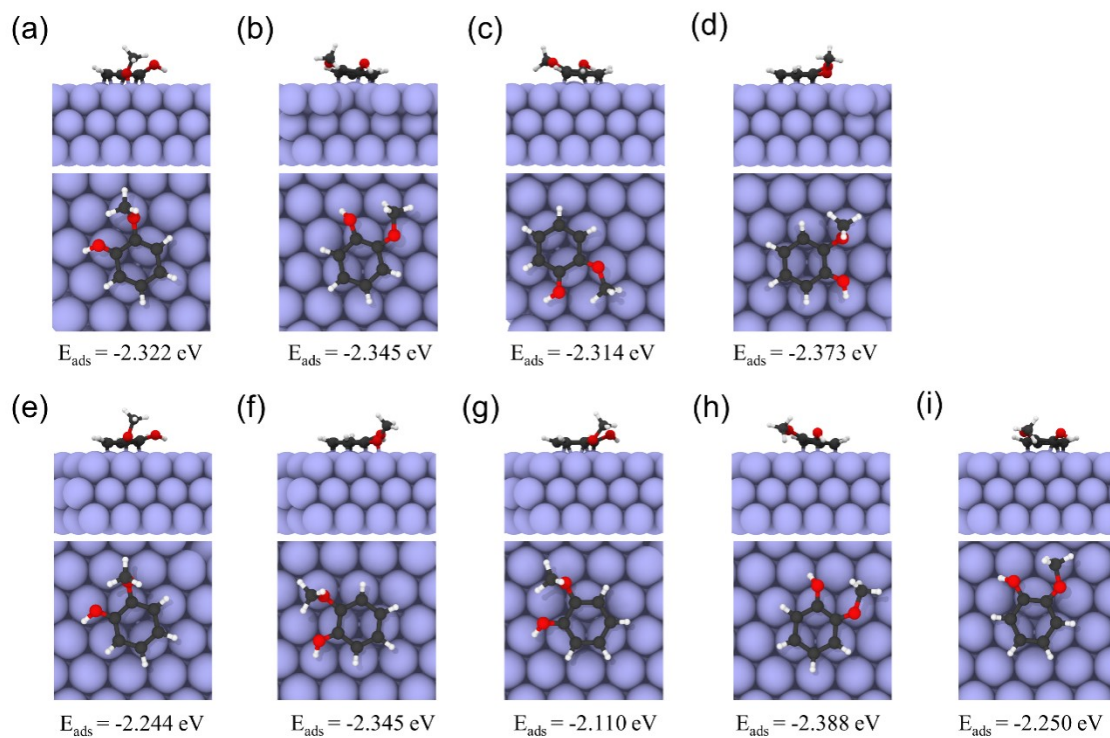


Figure S1. Possible adsorption sites of Guaiacol compound at the Ni (111) surface.

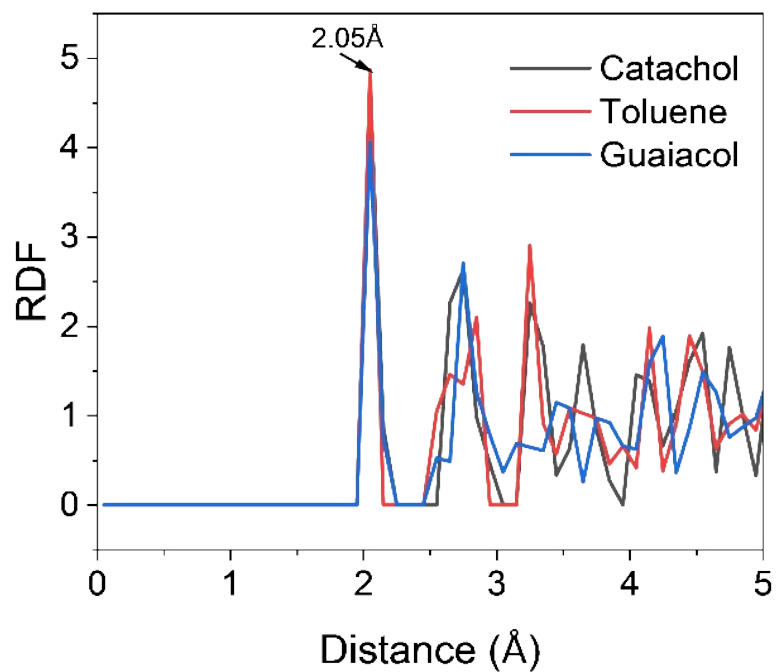


Figure S2. The radial distribution function of the optimal adsorption configuration of aromatic hydrocarbon benzene ring carbon atoms on the surface, guaiacol, toluene, and catechol.

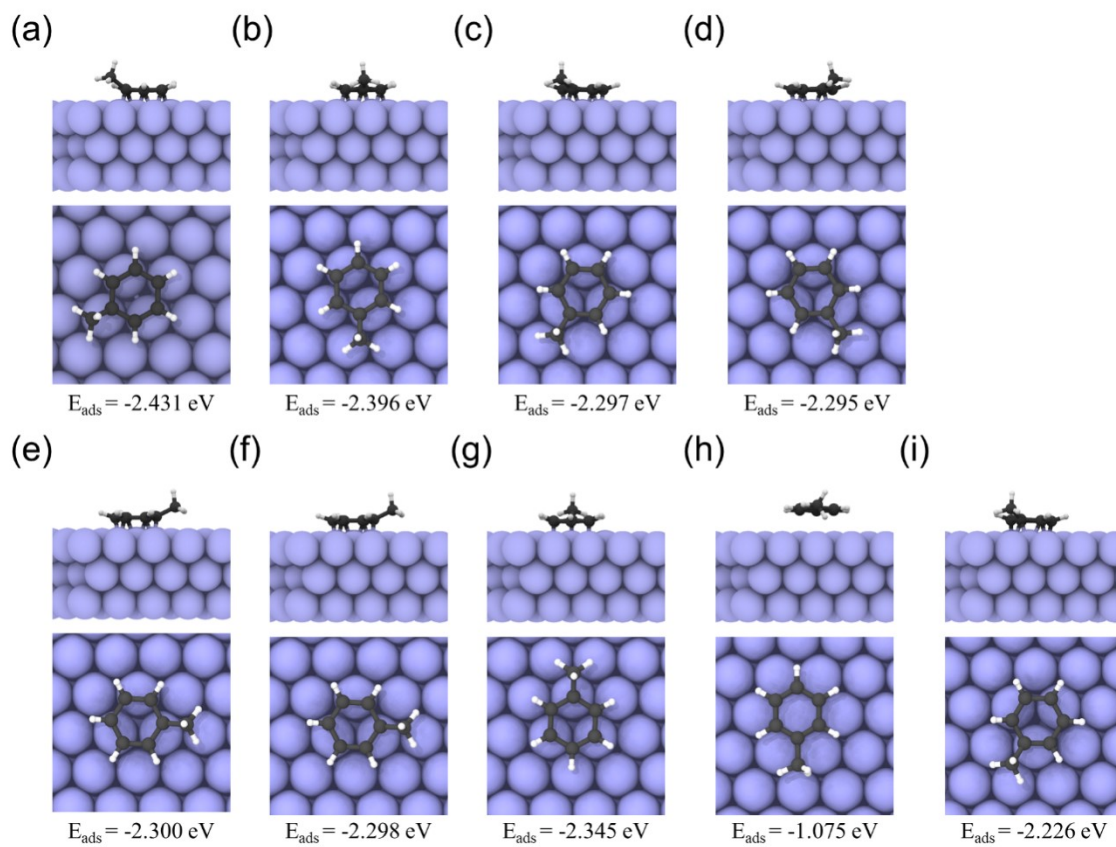


Figure S3. Possible adsorption sites of toluene compound and corresponding adsorption energies at the Ni (111) surface.

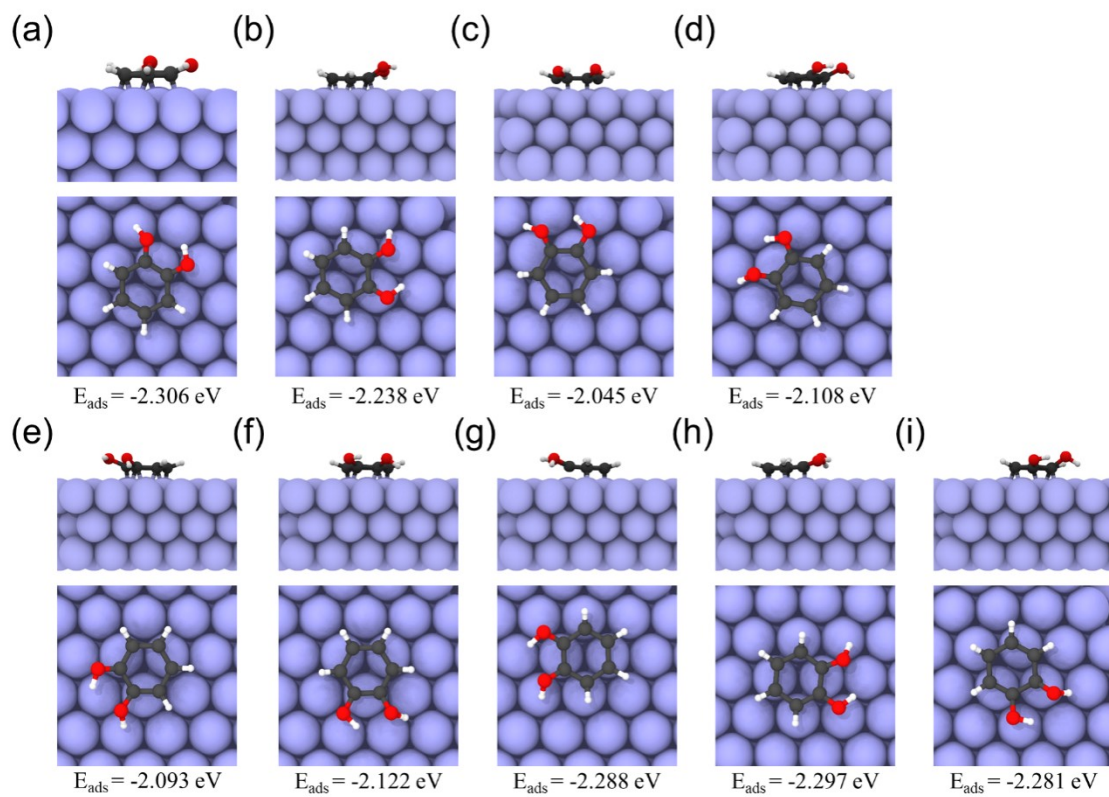


Figure S4. Possible adsorption sites of catechol compound and corresponding adsorption energies at the Ni (111) surface.

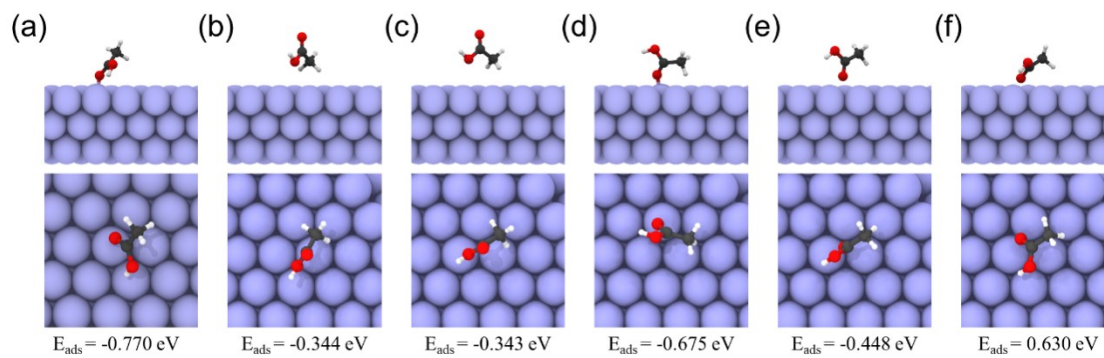


Figure S5. Possible adsorption sites of acetic acid compound and corresponding adsorption energies at the Ni (111) surface.

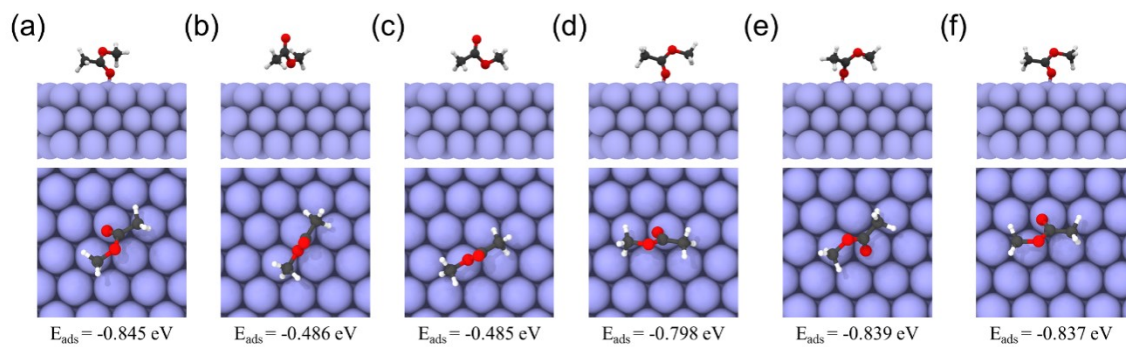


Figure S6. Possible adsorption sites of methyl acetate compound and corresponding adsorption energies at the Ni (111) surface.

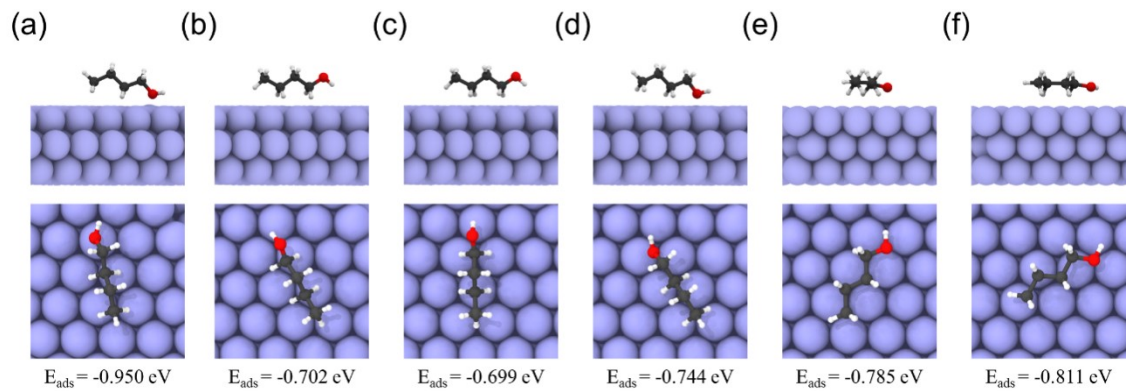


Figure S7. Possible adsorption sites of N-butanol compound and corresponding adsorption energies at the Ni (111) surface.

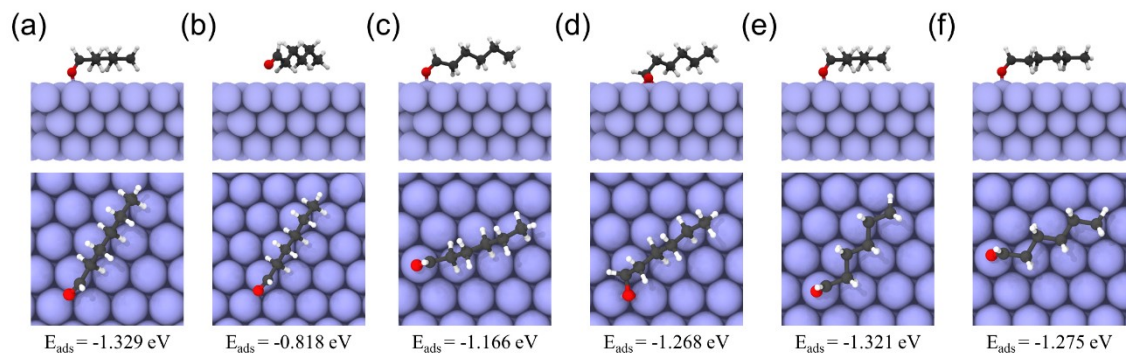


Figure S8. Possible adsorption sites of N-hexanal compound and corresponding adsorption energies at the Ni (111) surface.

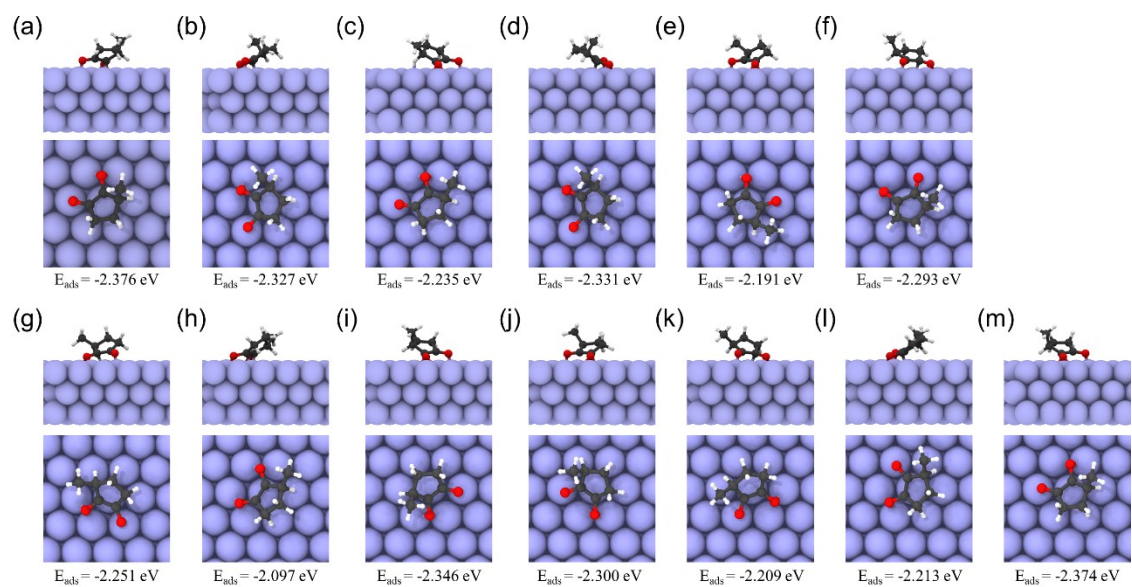


Figure S9. Possible adsorption sites of cyclopentanedione compound and corresponding adsorption energies at the Ni (111) surface.

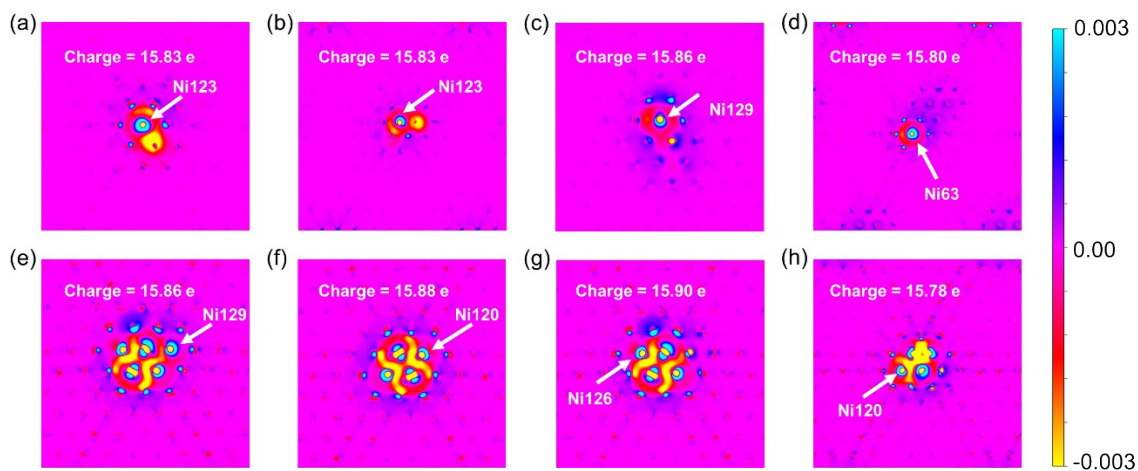


Figure S10. Calculated electron localization function (ELF) of polarized Ni atoms for different adsorption systems: (a) acetic acid, (b) methyl acetate, (c) N-butanol, (d) N-hexanal, (e) guaiacol, (f) toluene, (g) catechol, and (h) cyclopentanedione.

Table S1. Calculated adsorption energies for oxygen-containing organic monomers on Ni(111) surfaces relative to gas-phase compounds in this work and previous studies, ΔE in eV.

| Molecule | Previous studies | GGA-PBE this work |
|-------------------|---|-------------------|
| N-butanol | - | -0.950 |
| HAc | -0.518 ^{a,b} | -0.770 |
| Methyl acetate | - | -0.845 |
| N-hexanal | - | -1.329 |
| Toluene | - | -2.431 |
| Catechol | -1.78 ^c , -1.83 ^d | -2.306 |
| Guaiacol | -1.80 ^c , -1.76 ^d | -2.388 |
| Cyclopentanedione | - | -2.376 |

^a Cheah et al.¹, ^b Shi et al.², ^c Morteo-Flores et al.³, ^d Liu et al.⁴

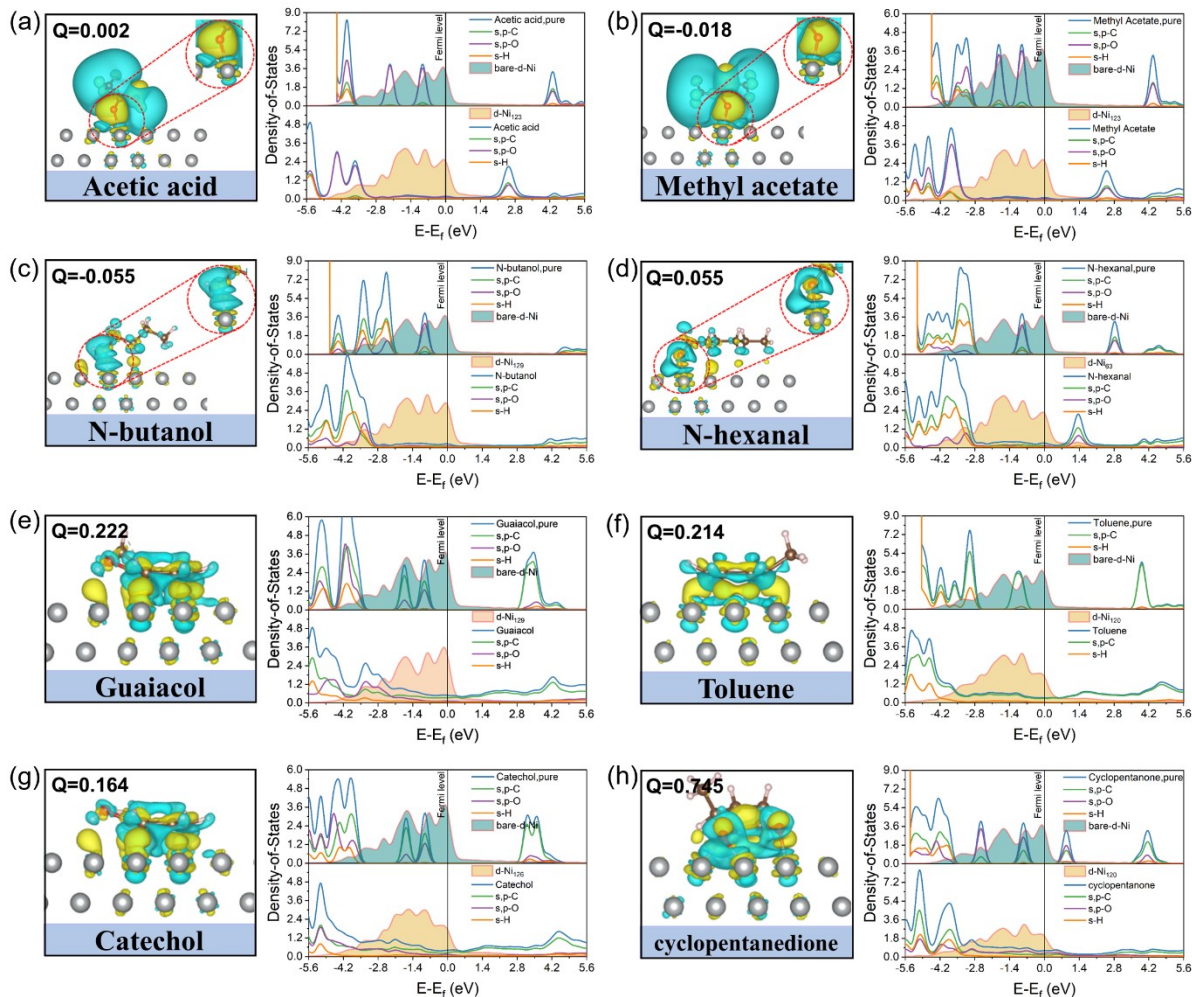


Figure S11. Calculated Electron density difference (EDD) (left maps), total density of states (TDOS) of the pure-substrates and adsorbates, and partial density of states (PDOS) of the Ni atoms that lose the most electrons (right curves). The zero energy (vertical dashed line) is set to the Fermi level. The surfaces correspond to a density difference of 0.0015 a.u. for chain compounds and 0.003 a.u. for cyclic compounds; Yellow and cyan areas indicate positive and negative electron densities. Q represents charge transfer.

Charge transfers are calculated based on the Bader charge analysis. We are exclusively concerned with the localized orbital interactions and charge transfer behaviors of organic species adsorbed

on Ni (111) surface at specific sites. Therefore, we selected the Ni atom on the Ni (111) surface with the highest electron loss as the site where the chemical reaction occurs, as shown in **Fig.S10**. The contributions of Ni atoms to the orbitals mainly arise from the 3d orbitals. For acetic acid, the molecular orbital contributions come from the s and p orbitals of oxygen atoms, and the antibonding orbitals derive from C and O atoms. From the EDD mapping, it can be observed that the electron-rich regions are around the carbonyl oxygen atom and at the upper end of the Ni atom (**Fig.S11(a, b, d, h)**, yellow isosurfaces), whereas there exists an electron-depleted region between the oxygen and Ni atoms (blue isosurfaces). This implies the transfer of electrons from the Ni slab to the oxygen atom, resulting in a significant charge accumulation region between Ni and O atoms. Furthermore, both before and after adsorption, there is substantial overlap between the s and p orbitals of oxygen atoms near the Fermi level and the 3d orbitals of Ni. After hybridization with the d orbitals, the energy of the s and p orbitals of oxygen atoms near the Fermi level decreases, while the density of states of Ni's 3d orbitals near the Fermi level decreases. This indicates a strong σ^* -d interaction between the carbonyl oxygen and Ni, forming a stable adsorption structure. However, for hydroxyl oxygen (**Fig.S11c**), after adsorption, the σ -bonding orbitals show differentiation. The energy decrease of the oxygen atom's TDOS is slightly smaller than that of the overall molecular TDOS. Moreover, there is a significant electron dissipation between hydroxyl oxygen and Ni, preventing Ni and oxygen from forming covalent interactions. Meanwhile, a Bader charge analysis was employed to investigate the charge transfer during the adsorption of bio-oil components on the Ni surface. The total charge transfer between the Ni surface and the aliphatic compounds is very small (-0.055 to -0.055 e), possibly due to the counterbalance between the electron enrichment of oxygen atoms and the electron dissipation of hydrogen atoms. Significant changes in electron density occur between Ni atoms and aromatic rings (large yellow regions

between the substrate and the surface), indicating the presence of d- π interactions. The TDOS of toluene molecules is primarily contributed by carbon atoms on the benzene ring. The hybridization between bonding π orbitals near the Fermi level and π^* antibonding orbitals above the Fermi level with Ni's 3d orbitals leads to delocalization, and the energy of the π^* antibonding orbitals increases. Charge transfer in the aromatic system is relatively significant. For 3-methyl-1,2-cyclopentanedione, similar to the aliphatic compounds, there is clear electron distribution between the carbonyl oxygen and Ni atoms. The Ni atom experiences the largest electron loss ($q = 15.78$ e, **Fig.S10**), with a total charge transfer of 0.745 e, leading to more electrons filling the antibonding orbitals, causing the disappearance of antibonding orbitals above the Fermi level. In total, the C or O s,p TDOS adsorbed on the bare slab at energies just below the Fermi level is transferred to lower energies, where Ni and components orbitals strongly hybridize. All of these indicate that the electrons of the adsorbate occupy more low energy states after adsorption.

Charge Calculation Algorithm

In addition to valence interactions, which model the interactions between overlapping orbitals, non-covalent interactions also play a crucial role. The fluctuating charge model is employed to describe electrostatic and polarization interactions. ReaxFF includes an energy term for fluctuating charges, which are re-optimized for every new geometry. The electronegativity equalization method (EEM) was followed by Eq.(1):

$$E_{EEM} = \min_{q_i: \sum q_i = q_{tot}} \left[\sum_{i=1}^{natom} \chi_i q_i + \frac{1}{2} \sum_{i=1, j=1}^{natom} \text{Tap}(r_{ij}) \frac{1}{4\pi \epsilon_0} \frac{q_i \cdot q_j}{\left[r_{ij}^3 + (\gamma_i \gamma_j)^{-3/2} \right]^{1/3}} q_i q_j \right] \quad (1)$$

Where the EEM energy contains the following ingredients: q_i is atomic charge, q_{tot} represents total charge, $\text{Tap}(r_{ij})$ represents Taper correction, r_{ij} represents interatomic distance, γ_i represents atomic short-range damping constant for electrostatic interactions, χ_i represents intrinsic atomic electronegativity, and the $\frac{1}{4\pi \epsilon_0}$ item has a value of 332.0638.

The existence of a unique chemical potential everywhere in the molecule establishes the electronegativity equalization principle, which demands that $\chi_\alpha = \chi_\beta = \chi_\gamma = \dots$ apply for all atoms α , β , γ , etc, in the molecule, as followed in Eq.(2):

$$\chi_\alpha = (\chi_\alpha^o + \Delta\chi_\alpha) + 2(\eta_\alpha^o + \Delta\eta_\alpha)q_\alpha + \sum_{\beta \neq \alpha} \frac{q_\beta}{R_{\alpha\beta}} \quad (2)$$

Where χ_α^o and η_α^o are the neutral atom electronegativity and hardness, respectively, q_α and q_β are the charges on atoms α and β , and $R_{\alpha\beta}$ is the internuclear distance. The $\Delta\chi_\alpha$ and $\Delta\eta_\alpha$ are the corrections to the value of χ_α^o and η_α^o . The electronegativity χ and the hardness η for most atoms are available from Sanderson⁶ and Parr⁷ and Pearson scales, respectively, and are used in the EEM method.

The ReaxFF parameter files provided were created using a charge equilibration (QEq) model for handling the electrostatic interactions following the procedures described in Rappe and Goddard^{8,9} and formulated in Nakano¹⁰. The QEq method minimizes the electrostatic energy of the system by adjusting the partial charge on individual atoms based on interactions with their neighbors. At each MD time step, the atomic charges q_i are determined to minimize the electrostatic energy $E_{EM}(\{\mathbf{x}_i(t)\}, \{q_i\})$, subject to the charge-neutrality constraint $\sum_i q_i = 0$.

References

1. Ezeonu, L.; Tang, Z.; Qi, Y.; Huo, F.; Zheng, Y.; Koel, B. E.; Podkolzin, S. G., Adsorption, surface reactions and hydrodeoxygenation of acetic acid on platinum and nickel catalysts. *Journal of Catalysis* **2023**, *418*, 190-202.
2. Shi, H.; Xia, M.; Lu, H.; Xie, Q.; Jia, L.; Hou, B.; Xiao, Y.; Li, D., Theoretical investigation of the reactivity of flat Ni (111) and stepped Ni (211) surfaces for acetic acid hydrogenation to ethanol. *International Journal of Hydrogen Energy* **2021**, *46* (29), 15454-15470.
3. Morteo-Flores, F.; Roldan, A., Mechanisms and Trends of Guaiacol Hydrodeoxygenation on Transition Metal Catalysts. *Frontiers in Catalysis* **2022**, *2*.
4. Liu, X.; An, W.; Wang, Y.; Turner, C. H.; Resasco, D. E., Hydrodeoxygenation of guaiacol over bimetallic Fe-alloyed (Ni, Pt) surfaces: reaction mechanism, transition-state scaling relations and descriptor for predicting C–O bond scission reactivity. *Catalysis Science & Technology* **2018**, *8* (8), 2146-2158.
6. Sanderson, R., *Chemical Bonds and Bond Energy*, NY: Acad. Press: 1976.
7. Parr, R. G.; Pearson, R. G., Absolute hardness: companion parameter to absolute electronegativity. *Journal of the American Chemical Society* 1983, *105* (26), 7512-7516.
8. Aktulga, H. M.; Fogarty, J. C.; Pandit, S. A.; Grama, A. Y., Parallel reactive molecular dynamics: Numerical methods and algorithmic techniques. *Parallel Computing* 2012, *38* (4), 245-259.
9. Rappe, A. K.; Goddard, W. A., Charge equilibration for molecular dynamics simulations. *The Journal of Physical Chemistry* 1991, *95* (8), 3358-3363.
10. Nakano, A., Parallel multilevel preconditioned conjugate-gradient approach to variable-charge molecular dynamics. *Computer Physics Communications* 1997, *104* (1), 59-69.

